

ARTICLE

Received 5 Jul 2013 | Accepted 21 Nov 2013 | Published 7 Jan 2014

DOI: 10.1038/ncomms3983

# Photoactuators and motors based on carbon nanotubes with selective chirality distributions

Xiaobo Zhang<sup>1,2,3</sup>, Zhibin Yu<sup>1,2,3</sup>, Chuan Wang<sup>1,2,3</sup>, David Zarrouk<sup>1</sup>, Jung-Woo Ted Seo<sup>4</sup>, Jim C. Cheng<sup>1,2</sup>, Austin D. Buchan<sup>1</sup>, Kuniharu Takei<sup>1,2,3</sup>, Yang Zhao<sup>5</sup>, Joel W. Ager<sup>3</sup>, Junjun Zhang<sup>1,2,3</sup>, Mark Hettick<sup>1,2,3</sup>, Mark C. Hersam<sup>4</sup>, Albert P. Pisano<sup>2,5</sup>, Ronald S. Fearing<sup>1</sup> & Ali Javey<sup>1,2,3</sup>

Direct conversion of light into mechanical work, known as the photomechanical effect, is an emerging field of research, largely driven by the development of novel molecular and polymeric material systems. However, the fundamental impediment is that the previously explored materials and structures do not simultaneously offer fast and wavelength-selective response, reversible actuation, low-cost fabrication and large deflection. Here, we demonstrate highly versatile photoactuators, oscillators and motors based on polymer/single-walled carbon nanotube bilayers that meet all the above requirements. By utilizing nanotubes with different chirality distributions, chromatic actuators that are responsive to selected wavelength ranges are achieved. The bilayer structures are further configured as smart 'curtains' and light-driven motors, demonstrating two examples of envisioned applications.

<sup>1</sup>Electrical Engineering and Computer Sciences, University of California, Berkeley, California 94720, USA. <sup>2</sup>Berkeley Sensor and Actuator Center, University of California, Berkeley, California 94720, USA. <sup>3</sup>Materials Sciences Division, Lawrence Berkeley National Laboratory, Berkeley, California 94720, USA. <sup>4</sup>Materials Science and Engineering, Northwestern University, Evanston, Illinois 60208, USA. <sup>5</sup>Mechanical Engineering, University of California, Berkeley, California 94720, USA. Correspondence and requests for materials should be addressed to A.J. (email: ajavey@eecs.berkeley.edu).

Reconfigurable materials that change their shape and functionality in response to external stimuli represent a novel class of materials that enable new applications<sup>1–7</sup>. Previous work includes shape-reconfigurable structures based on shape memory polymers<sup>8,9</sup>, bimorphs<sup>10,11</sup>, molecular motors<sup>12–14</sup> and hydrogels<sup>15,16</sup> that respond to light or heat. For example, azobenzene functional materials have been utilized for photoactuators based on *cis–trans* transformation driven by light irradiation<sup>12,17,18</sup>. However, the need for dual wavelength operation (UV and visible) for reversible actuation and slow response time ( $\sim 10$  s) limit their practical utility for certain applications<sup>12,17,18</sup>. Recently, nanotube-based photoactuation has been reported using different platforms, including bilayers<sup>19</sup>, composites<sup>20</sup> and cantilever structures<sup>21</sup>, showing the promise of nanotubes for such applications. The principle actuation mechanism for most of these reported devices has been attributed to photo-induced charge build-up at the interfaces.

Here, we present a simple photoactuator device concept based on single-walled carbon nanotube (SWNT)/polymer bilayers that takes advantage of the highly intriguing photothermal properties

of SWNTs. The actuators deliver large deflection, fast ( $\sim 0.5$  s) and user-defined, wavelength-selective response. Previous studies have utilized the strong optical absorbance of SWNTs<sup>22</sup> in the near-infrared regime to induce significant local heating for photothermal cancer therapy. Furthermore, recent developments in the chirality purification of SWNTs have enabled the design of materials with desirable absorption properties and selective spectral response<sup>23–25</sup>. Building on these advancements, here we report a new class of highly versatile photoactuators based on SWNTs, with potential applications in smart curtains for energy-efficient windows, camouflage, sun-driven motors and oscillators, and monochromatic light sensors.

## Results

**Polymer/SWNT bilayers.** Figure 1a schematically illustrates the fabrication process of polymer/SWNT bilayers. The process is facile and scalable, which only involves vacuum filtration of a SWNT solution on a 10- $\mu\text{m}$ -thick polycarbonate (PC) membrane (0.4  $\mu\text{m}$  pore size). An optical image of a fabricated PC/SWNT

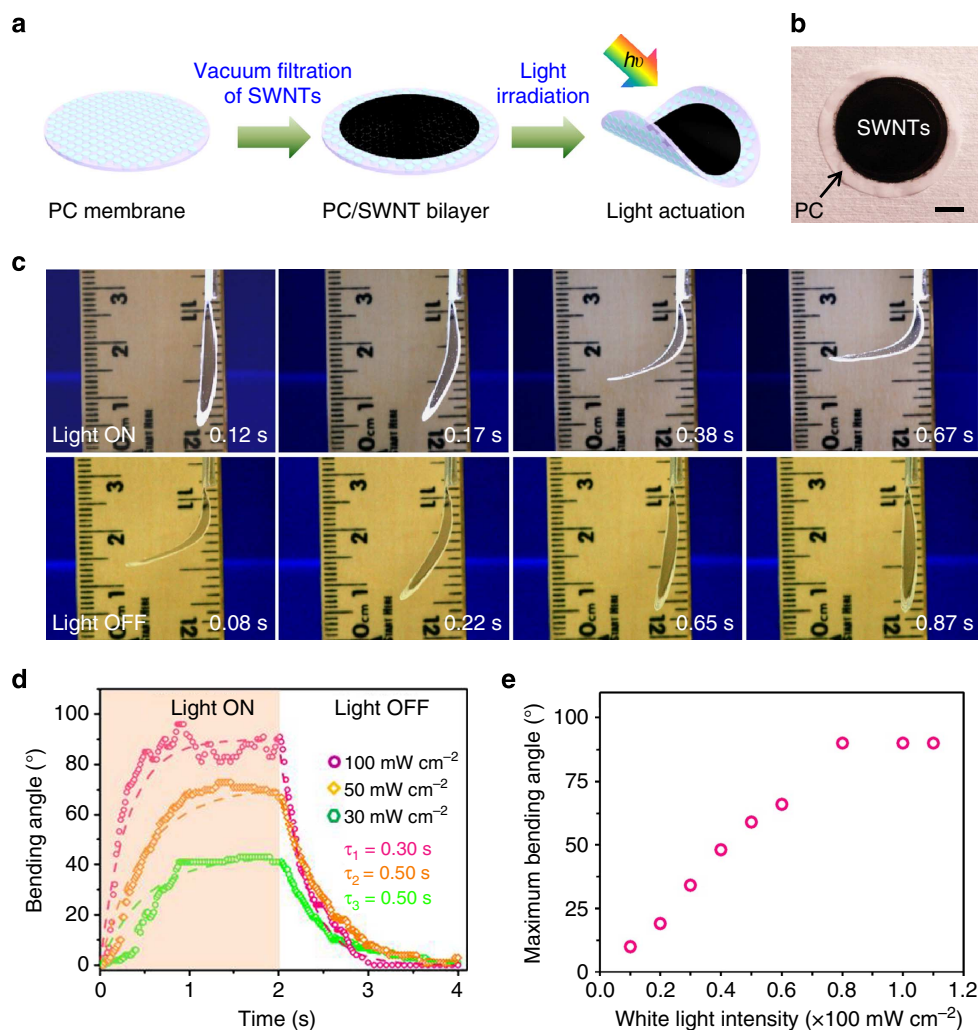


**Figure 1 | PC/SWNT bilayer photoactuators.** (a) Schematics illustrating the PC/SWNT bilayer structure. (b) Optical image of a circular PC/SWNT (10  $\mu\text{m}$ /1  $\mu\text{m}$  in thickness) bilayer with a diameter of 25 mm made by vacuum filtration (scale bar, 5 mm). (c) Series of optical images showing the light-actuation process of a bilayer structure with HiPCO nanotubes. The sample is held in air from the top edge, and illuminated with 100- $\text{mW cm}^{-2}$  white light normal to its surface (light is incident from the left side). The first and second row images correspond to the bending (light on) and unbending (light off) processes, respectively. (d) Bending angle as a function of time as light is turned on (time, 0 s) and off (time, 2 s) for different illumination intensities. The circle data points are from experiments, and the dashed lines represent the exponential fits. (e) Maximum (i.e., steady state) bending angle as a function of solar light intensity.

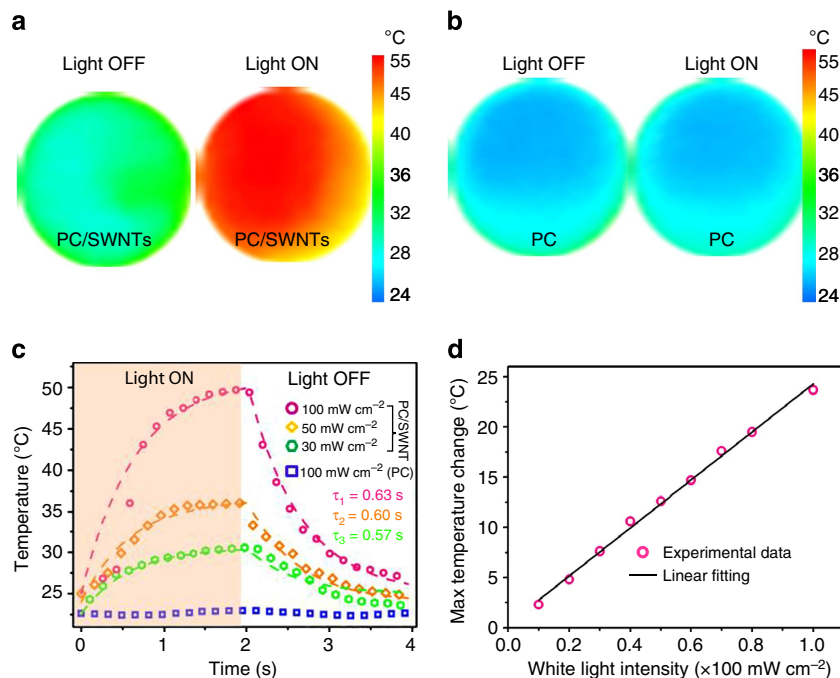


**Figure 2 | Photothermal characterization of PC/SWNT bilayers.** (a) Infrared images of a PC/SWNT bilayer with and without light illumination ( $100 \text{ mW cm}^{-2}$ , white light). (b) Infrared images of a blank PC film used as a control with and without light illumination ( $100 \text{ mW cm}^{-2}$ ). (c) Temperature measurements of a PC/SWNT bilayer as light is turned on (time, 0 s) and off (time, 2 s) for different illumination intensities. (d) Maximum temperature rise of the PC/SWNT bilayer as a function of solar light intensities. For panels a–d HiPCO nanotubes were used with a film thickness of  $1 \mu\text{m}$ .

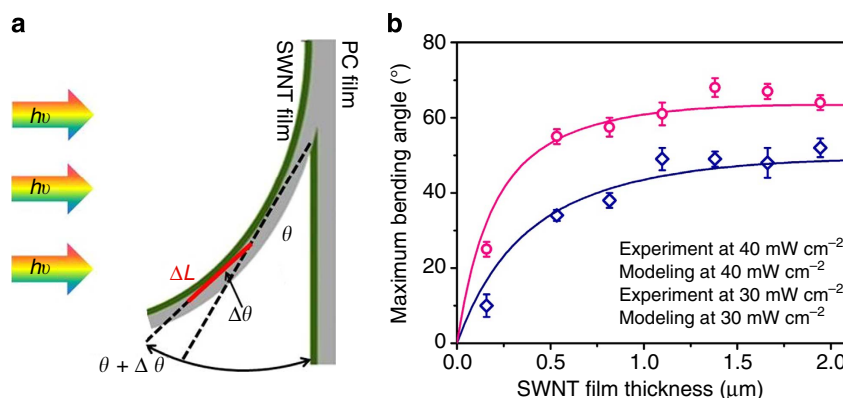


**Figure 3 | Mechanical modelling of PC/SWNT actuators.** (a) A bilayer model used in the mechanical simulation. Because of the difference in coefficient of thermal expansion, a bilayer PC/SWNT structure with a length  $L$  is deflected to a curvature radius of  $R$  and bending angle of  $\theta$  when heated by light illumination. Here, the edge of the structure is fixed in position, similar to those of the actuator experiments. (b) Modelling and experimental results for the maximum bending angle as a function of SWNT film thickness. The thickness of the PC layer is fixed at  $10 \mu\text{m}$ .

bilayer structure is shown in Fig. 1b. The SWNTs form densely packed thin films on top of the PC membrane as seen from the scanning electron microscopy images in Supplementary Fig. S1. The thickness of the SWNT thin-film is controlled from  $\sim 0.2$  to  $2 \mu\text{m}$  by adjusting the total amount of the filtered SWNTs (Supplementary Fig. S2). Three types of nanotubes were explored: HiPCO, metal-enriched and (6,5) chirality-enriched SWNTs. In this bilayer structure, the SWNTs serve as an excellent light absorber layer with the specific wavelength range of absorption dependent on the type of nanotubes used<sup>26</sup>. The absorbed photon energy in nanotubes is readily converted to heat, which is then transported to the PC layer. The vacuum filtration ensures a mechanically coherent SWNTs/PC interface for effective heat

transfer between the two layers. As the PC membrane has a large coefficient of thermal expansion of  $\sim 65$  p.p.m. per Kelvin<sup>27</sup>, which is over  $10 \times$  larger than that of SWNTs ( $< 4$  p.p.m. per Kelvin)<sup>28</sup>, the structure is strongly curled (that is, deflected) towards the SWNT side upon light irradiation (Fig. 1a, right panel).

**Photoresponse of bilayer actuators.** The fast and reversible photoactuation of the PC/SWNT structures is evident from the optical photographs shown in Fig. 1c. Here, HiPCO nanotubes are used<sup>29</sup>. When the PC/SWNT bilayer is placed directly under a solar simulator with 1-sun intensity ( $100 \text{ mW cm}^{-2}$ ), the sample

is bent  $\sim 90^\circ$  within  $\sim 0.67$  s and reverts back to the relaxed (that is, flat) state in  $\sim 0.87$  s after the light is turned on and off, respectively. By using a high-speed video camera (1,200 frames per second), the bending angle of the actuator is captured and plotted as a function of time for different illumination intensities (Fig. 1d).

The bending and unbending processes can both be fitted with an exponential response using equations (1) and (2):

$$\theta = \theta_0 \left[ 1 - \exp\left(-\frac{t}{\tau}\right) \right] \text{ for bending;} \quad (1)$$

$$\theta = \theta_0 \exp\left(-\frac{t}{\tau}\right) \text{ for unbending} \quad (2)$$

where  $\theta_0$  is the maximum bending angle,  $t$  is time and  $\tau$  is the actuation response time constant. The actuation response time constant is extracted to be  $\sim 0.50$  s for both bending and unbending, which is significantly faster than the azobenzene-based polychromic materials with a response time of  $\sim 10$  s<sup>12</sup>.

The fast response is attributed to the low heat capacity<sup>30</sup>, high thermal conductivity (Supplementary Fig. S3)<sup>31</sup> and the excellent near-infrared light absorption of the SWNT thin film<sup>32</sup>, making them ideal photothermal material.

Owing to the superb optical absorbance properties of SWNTs, the PC/SWNT photothermal actuator is highly sensitive to light irradiation. Figure 1e exhibits the maximum bending angle as a function of the light intensity; an easily detectable bending angle of  $\sim 10^\circ$  is found at  $10 \text{ mW cm}^{-2}$  (0.1 sun). The bending angle starts to saturate at  $\sim 90^\circ$  when the illumination intensity is  $> 80 \text{ mW cm}^{-2}$  (0.8 sun). Interestingly, further increase of the intensity causes the structure to oscillate around its saturation bending angle ( $90^\circ$ ) due to the shadowing effect. Specifically, as the bending angle becomes slightly larger than  $90^\circ$ , part of the SWNT film becomes blocked from light irradiation due to self-shadowing, hence driving the oscillation process. This phenomenon is depicted in the Supplementary Movie 1, where an oscillation frequency of  $\sim 5$  Hz is observed for continuous 1.2-sun illumination.

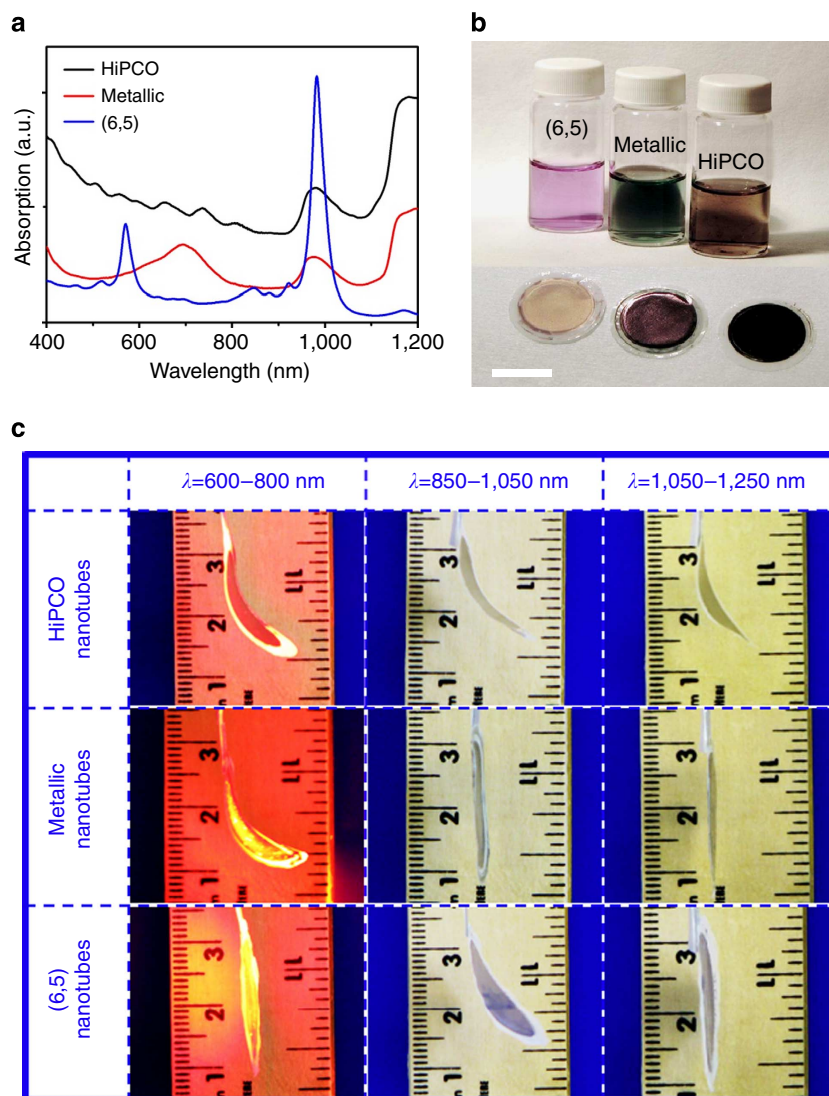


**Figure 4 | Chromatic photoactuators made from nanotubes with different chirality distributions.** (a) Optical absorption spectra for HiPCO, metallic and (6,5)-enriched nanotube films. (b) Optical image of the bilayer structures made from HiPCO, metallic, and single-chirality-enriched nanotubes along with their corresponding nanotube solutions (scale bar, 15 mm). (c) Light response of the three different bilayers from panel b for wavelength bands of 600–800 nm, 850–1,050 nm and 1,050–1,250 nm. For each wavelength band, the power is calibrated to maintain the same transmitted power of  $\sim 35 \text{ mW cm}^{-2}$ . Light is incident from the right side of the image, normal to the surface of the samples.

**Photothermal actuation mechanism.** To elucidate the underlying photothermal mechanism of the PC/SWNT bilayers, we used an infrared camera to measure the real-time temperature change of the sample upon light irradiation (see Methods for details of the set-up). Figure 2a shows the temperature profile of a PC/SWNT bilayer film (10  $\mu\text{m}/1 \mu\text{m}$ ) when the light is on and off. It is evident that the temperature of the substrate is increased by  $\sim 20^\circ\text{C}$  under 1-sun illumination. In contrast, no observable temperature change is found in the PC film without SWNTs (Fig. 2b). Figure 2c shows the temperature of a PC/SWNT bilayer as a function of exposure time to light with various illumination intensities. Rapid temperature rise and decay are clearly observed. A thermal time constant (corresponding to 63% drop in temperature) of  $\sim 0.60$  s is extracted similar to Fig. 1d. This extracted thermal time constant is close to the actuation response time constant (Fig. 1d), which confirms the underlying photothermal actuation mechanism. As shown in Fig. 2d, the maximum temperature change and light intensity show near-linear dependency. The comparison between Figs 1e and 2d indicates that a  $5^\circ\text{C}$  change in the temperature (corresponding to  $20 \text{ mW cm}^{-2}$  illumination) results in a bending angle of  $\sim 20^\circ$ , depicting the high sensitivity of the system. The photothermal effect of PC/SWNT bilayers with various SWNT layer thicknesses was also investigated and summarized in Supplementary Table S1. We also carried out control experiments inside an oven to induce pure thermal actuation. The bending angle measurements from these control experiments are consistent with the photoactuation experiments for the same temperature change as shown in Supplementary Fig. S4 and Supplementary Table S2.

Next, we focus on understanding the time-limiting step in the actuation of our bilayers by calculating the thermal time constant of both SWNT and PC films (Supplementary Note 1). First, we estimated the average heat transfer coefficient of free air convection of the two surfaces of PC/SWNT from the equilibrium

temperature change under solar light irradiation according to the following equation:  $2h\Delta T = W_{\text{in}}$ . Here,  $h$  is the average heat transfer coefficient,  $\Delta T$  is the equilibrium temperature change and  $W_{\text{in}}$  is the power density of solar irradiation. The estimated heat transfer coefficient is  $20.6 \text{ W m}^{-2} \text{ K}^{-1}$ . The thermal time constant is then calculated according to  $\tau = \rho C b / h$ , where  $\rho$  is mass density of the film;  $C$  is the specific heat;  $b$  is the thickness of the film. The calculated thermal time constants of the SWNT and PC films are 0.04 and 0.7 s, respectively. Clearly, the heat capacity in the PC layer dominates the response time with the calculated value matching the experiments well, suggesting that the proposed operation mechanism is indeed viable (Fig. 2c).

**Mechanical modelling.** Mechanical modelling was performed to quantitatively study the effect of SWNT film thickness and the maximum temperature change on the static maximum bending angle (Fig. 3). The sample receives non-uniform illumination due to mechanical curling of the actuator (Fig. 3a). Based on the bimetal thermostat equation of Timoshenko<sup>33</sup>, we developed an analytical model for the bending angle with non-uniform light irradiation (Supplementary Note 2). From modelling, the effect of SWNT film thickness (PC thickness of  $10 \mu\text{m}$ ) on the maximum bending angle for a given illumination intensity is calculated. The modelling matches the experimental results well (Fig. 3b). The maximum deflection increases with SWNT film thickness up to  $\sim 1 \mu\text{m}$ , beyond which further increase in the SWNT thickness has minimal effect. The results show that a high degree of control in the dynamic range of our bilayer actuators can be obtained by simply tuning the thickness of the SWNT film as compared with that of the PC substrate. The conversion efficiency of our actuators (defined as the generated elastic energy due to photoactuation divided by the incident light energy) is estimated to be  $\sim 0.01\%$  (Supplementary Note 3). It is noted

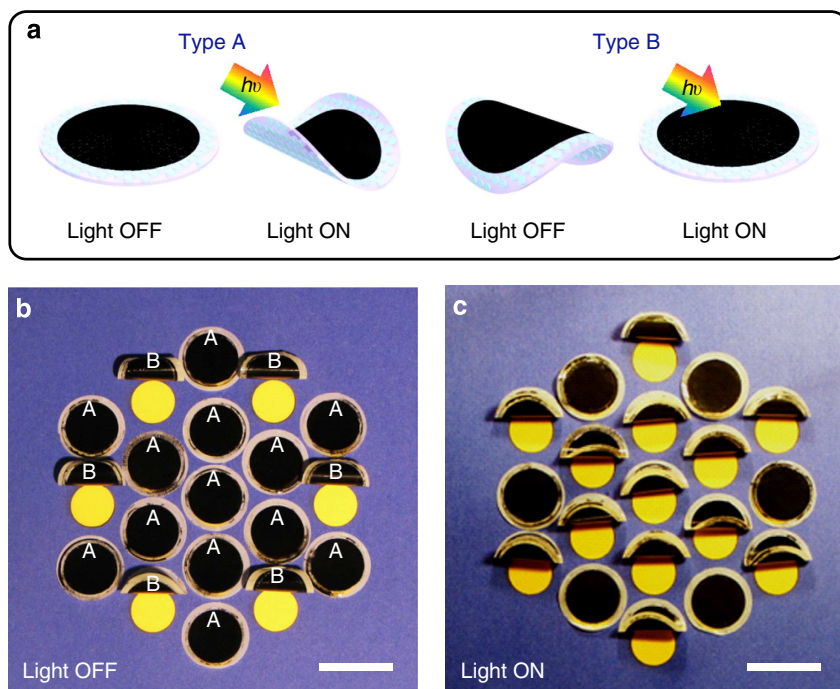


**Figure 5 | Smart curtains.** (a) Schematic for two different types of PC/SWNT photoactuators made by tuning the built-in strain of the bilayers. Type A is flat (that is, closed) in the absence of sunlight and is curled (that is, open) when exposed to sunlight. Type B is reversed (that is, open in the absence of light and closed under light). (b,c) Hexagonal array of 19 bilayer actuators (13 Type A and 6 Type B) when simulated sunlight is off and on, respectively. The circular actuators are mounted on a blue cardboard by their top edge only. The region underneath the actuators is marked yellow, so that when the actuators are open, the effect is clearly visible. Here, HiPCO nanotubes were used (scale bar, 25 mm).

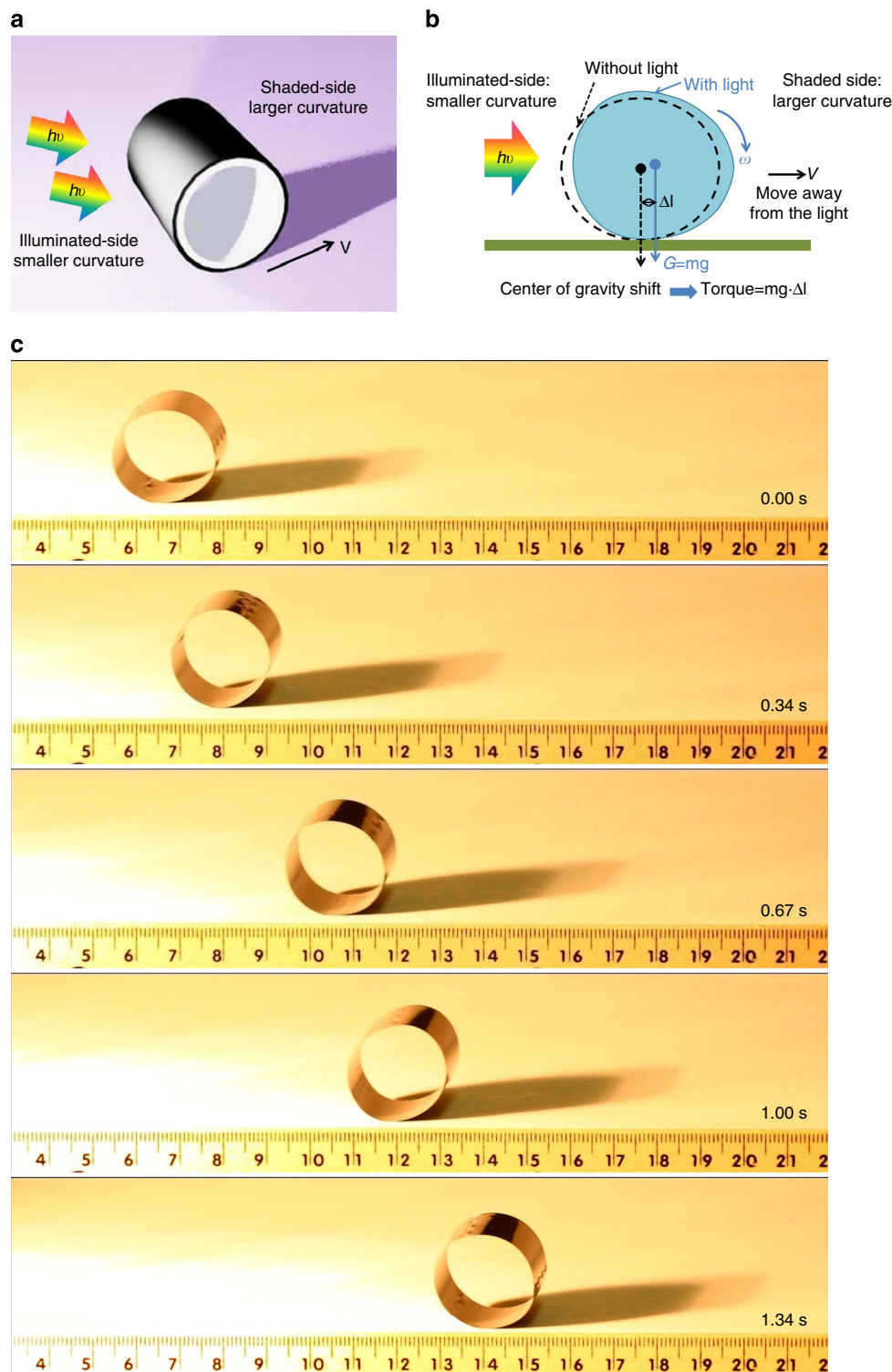


**Figure 6 | A fast forward-moving motor driven by light.** (a) Schematic showing the operation scheme of the motor under light. The motor consists of a PC/SWNT bilayer ( $25\mu\text{m}/1\mu\text{m}$  in thickness) that is rolled into a tubular structure (diameter of  $\sim 2$  cm; length of  $\sim 2.5$  cm). (b) Schematic showing the displacement in the center of gravity of the motor due to the directional light exposure. The induced torque drives the motor away from the light source. (c) Optical image series as a function of time showing a forward-moving motor driven by a halogen lamp.

that this energy conversion efficiency is for doing internal work on deforming the bilayer rather than for doing external work.

**User-defined, wavelength-selective response.** A unique feature of the PC/SWNT photothermal actuators is the tunability of the

responsive wavelength range by using nanotubes with different chirality distributions. It is known that the light absorption characteristics of carbon nanotubes are determined by their chiralities<sup>26</sup>. To demonstrate this feature, in addition to using as-synthesized HiPCO tubes with a mixture of chiralities, we used 98% purity metallic nanotubes (as-received from NanoIntegris)

with  $M_{11}$  absorption peak at  $\sim 700$  nm (average nanotube diameter of 1.4 nm), and (6,5) single-chirality nanotubes prepared as previously described<sup>24</sup> (purity > 97%) with  $S_{22}$  and  $S_{11}$  absorption peaks at  $\sim 560$  nm and 970 nm, respectively (Fig. 4a,b). For the light-actuation experiments, three illumination wavelength bands of 600–800 nm, 850–1,050 nm and 1,050–1,250 nm were created by using a combination of long- and short-pass optical filters. The power of the light source was calibrated to maintain the same transmitted power for all three wavelength bands. As expected, HiPCO nanotubes are responsive to all three wavelength bands (Fig. 4c). In contrast, the actuators with metal-enriched nanotubes are only responsive to the visible wavelength band of 600–800 nm. On the other hand, actuators with single-chirality (6,5) nanotubes only respond to the 850–1,050 nm band. The wavelength-dependent response is also evident from the photothermal measurements (Supplementary Fig. S5). This feature represents a useful and unique aspect of the actuators that takes advantage of the intriguing optical properties of nanotubes.

**Smart curtains.** Finally, we focus on the use of PC/SWNT actuators for practical applications. In one example, we demonstrate their use for ‘smart’ curtains that can be engineered to be either closed or opened upon sunlight illumination (Fig. 5). Here, circular PC/SWNT bilayers are mounted on a surface by their top edge only. Two types of bilayers based on HiPCO nanotubes are utilized (Fig. 5a). One involving the configuration discussed above, which curls up (that is, opens) on light illumination (Type A). The other operates in the reverse mode—that is being curled open in the absence of light and closing (that is, moving to the flat state) on light illumination (Type B). To fabricate Type B actuators, PC/SWNT bilayers are pre-strained at 70 °C for 12 h to make them curled to the PC side. By arraying the circular actuators on a stage with each actuator being mounted by the top edge, a curtain is obtained that either closes (Type B) or opens (Type A) by light illumination (Fig. 5b,c, and Supplementary Movie 2). Besides energy-efficient windows, this smart curtain may be potentially useful for camouflage applications.

**Motors and oscillators.** As a second application demonstration of PC/SWNT actuators, we have fabricated a 2-cm-sized motor, which rolls away from the direction of light illumination. The motor is fabricated by assembling three pieces of rectangular (2 cm  $\times$  2.5 cm) PC/SWNT (25  $\mu$ m/1  $\mu$ m) film together into a cylinder with the SWNT side facing outwards. As illustrated in Fig. 6a,b, non-uniform illumination on the motor from an angled light source causes the curvature to decrease on the light-facing side, that is, the location that gets more illumination has the tendency to be flattened. This causes a change to the centre of mass of the motor, thereby resulting in a torque that drives the motor away from light on a flat surface at a speed of  $\sim 6$  cm s<sup>-1</sup> (Fig. 6c and Supplementary Movie 3). On the other hand, an oscillating wheel is made by making a roller with elliptical cross-section. In this case, the structure leans forward and backward at a frequency of  $\sim 2$  Hz on light illumination (Supplementary Movie 4). These demonstrations illustrate macro-scale motors with fast mechanical motion driven by a single light source, which can only be realized with fast and reversible light-responsive materials. As cyclic lifetime is critically important for practical use, we have measured 60,000 cycles of actuation test on a PC/SWNT bilayer. The deformation remains unchanged as shown in Supplementary Fig. S6 and Supplementary Movie 5.

## Discussion

In summary, PC/SWNT bilayer photoactuators with highly unique light-responsive properties were fabricated using a facile and low-cost room-temperature process. The PC/SWNT bilayers simultaneously offer fast response, extreme light sensitivity, large deflection and reversible actuation. By using SWNTs with different chirality distributions, the responsive wavelength range of the actuators is readily programmed, enabling the development of chromic actuators. As a benchmark for fast and reversible light-responsive properties, a smart curtain and a fast-moving motor have been demonstrated to highlight two representative applications of the proposed bilayers. Moving forward, the bilayer actuators can be optimized in terms of SWNT and polymer thickness, and polymer Young’s modulus to achieve larger force output, depending on the application needs. By exploiting nanotube-printing strategies on polymer substrates, this work can be extended in the future to the fabrication of complex, reconfigurable structures using a scalable process scheme.

## Methods

**PC/SWNT bilayer fabrication.** Purified HiPCO SWNT powder is purchased from NanoIntegris Inc. (residual Fe catalyst < 15 wt%, diameter 0.8–1.2 nm, length 100–1,000 nm). A 0.5-mg ml<sup>-1</sup> aqueous solution of SWNTs is made using 2% sodium deoxycholate as surfactant. After 400 min of sonication (Crest Ultrasonics 275DA; power 9), large SWNT aggregates, non-SWNT carbonaceous impurities, and metal catalyst particles were removed by centrifuging the SWNT dispersion for 10 min with 13,000g rotation speed. Vacuum filtration is performed using a standard 25-mm set up with a PC membrane (Millipore, 0.4- $\mu$ m pore size, 25 mm diameter). After filtration, 20 ml water is added to rinse away the surfactant. A similar fabrication process is used to obtain actuators with metallic and (6,5)-enriched nanotubes (with a concentration of  $\sim 0.01$  mg ml<sup>-1</sup>). All three actuators have the same SWNT film thickness of  $\sim 1$   $\mu$ m by controlling the amount of SWNTs used for the filtration.

**Temperature measurements of the PC/SWNT bilayers.** For the infrared camera measurements, the entire edge of the sample is fixed onto a piece of cardboard with a 20-mm hole so that the sample is mostly suspended in air and thermally well insulated. The temperature of the SWNT film surface is measured by an infrared camera. The camera is 25 mm away from the sample with 30° detection angle with respect to the surface normal of the sample.

## References

1. Stuart, M. A. C. *et al.* Emerging applications of stimuli-responsive polymer materials. *Nat. Mater.* **9**, 101–113 (2010).
2. Yerushalmi, R., Scherz, A., van der Boom, M. E. & Kraatz, H. B. Stimuli responsive materials: new avenues toward smart organic devices. *J. Mater. Chem.* **15**, 4480–4487 (2005).
3. Otsuka, K. & Ren, X. Physical metallurgy of Ti-Ni-based shape memory alloys. *Prog. Mater. Sci.* **50**, 511–678 (2005).
4. Schild, H. G. Poly (N-isopropylacrylamide)-experiment, theory and application. *Prog. Polym. Sci.* **17**, 163–249 (1992).
5. Ilievski, F. *et al.* Soft robotics for chemists. *Angew. Chem. Int. Ed.* **50**, 1890–1895 (2011).
6. Brochu, P. & Pei, Q. B. Advances in dielectric elastomers for actuators and artificial muscles. *Macromol. Rapid Commun.* **31**, 10–36 (2010).
7. Halsey, T. C. Electrorheological fluids. *Science* **258**, 761–766 (1992).
8. Lendlein, A. & Kelch, S. Shape-memory polymers. *Angew. Chem. Int. Ed.* **41**, 2034–2057 (2002).
9. Liang, J. J. *et al.* Infrared-triggered actuators from graphene-based nanocomposites. *J. Phys. Chem. C* **113**, 9921–9927 (2009).
10. Park, S., An, J., Suk, J. W. & Ruoff, R. S. Graphene-based actuators. *Small* **6**, 210–212 (2010).
11. Gracias, D. H. *et al.* Fabrication of micrometer-scale, patterned polyhedra by self-assembly. *Adv. Mater.* **14**, 235–238 (2002).
12. Yu, Y. L., Nakano, M. & Ikeda, T. Directed bending of a polymer film by light. *Nature* **425**, 145–145 (2003).
13. Balzani, V. *et al.* Autonomous artificial nanomotor powered by sunlight. *Proc. Natl Acad. Sci. USA* **103**, 1178–1183 (2006).
14. Kobatake, S. *et al.* Rapid and reversible shape changes of molecular crystals on photoirradiation. *Nature* **446**, 778–781 (2007).
15. Zhang, X. B. *et al.* Optically- and thermally-responsive programmable materials based on carbon nanotube-hydrogel polymer composites. *Nano. Lett.* **11**, 3239–3244 (2011).

16. Yu, C. J. *et al.* Electronically programmable, reversible shape change in two- and three-dimensional hydrogel structures. *Adv. Mater.* **25**, 1541–1546 (2013).
17. Li, Y. B., He, Y. N., Tong, X. L. & Wang, X. G. Photoinduced deformation of amphiphilic azo polymer colloidal spheres. *J. Am. Chem. Soc.* **127**, 2402–2403 (2005).
18. Yu, H. F. & Ikeda, T. Photocontrollable liquid-crystalline actuators. *Adv. Mater.* **23**, 2149–2180 (2011).
19. Levitsky, I. A., Kanelos, P. T., Woodbury, D. S. & Euler, W. B. Photoactuation from a carbon nanotube – nafion bilayer composite. *J. Phys. Chem. B* **110**, 9421–9425 (2006).
20. Ahir, S. V. & Terentjev, E. M. Photomechanical actuation in polymer-nanotube composites. *Nat. Mater.* **4**, 491–495 (2005).
21. Lu, S. & Panchapakesan, B. Nanotube micro-optomechanical actuators. *Appl. Phys. Lett.* **88**, 253107 (2006).
22. Kam, N. W. S., O’Connell, M., Wisdom, J. A. & Dai, H. J. Carbon nanotubes as multifunctional biological transporters and near-infrared agents for selective cancer cell destruction. *Proc. Natl Acad. Sci. USA* **102**, 11600–11605 (2005).
23. Tu, X. M., Manohar, S., Jagota, A. & Zheng, M. DNA sequence motifs for structure-specific recognition and separation of carbon nanotubes. *Nature* **460**, 250–253 (2009).
24. Green, A. A. & Hersam, M. C. Nearly single-chirality single-walled carbon nanotubes produced via orthogonal iterative density gradient ultracentrifugation. *Adv. Mater.* **23**, 2185–2190 (2011).
25. Ghosh, S., Bachilo, S. M. & Weisman, R. B. Advanced sorting of single-walled carbon nanotubes by nonlinear density-gradient ultracentrifugation. *Nat. Nanotechnol.* **5**, 443–450 (2010).
26. Bachilo, S. M. *et al.* Structure-assigned optical spectra of single-walled carbon nanotubes. *Science* **298**, 2361–2366 (2002).
27. Choy, C. L. *et al.* Thermal conductivity and thermal expansivity of in situ composites of a liquid crystalline polymer and polycarbonate. *Polym. Eng. Sci.* **36**, 827–834 (1996).
28. Jiang, H., Liu, B., Huang, Y. & Hwang, K. C. Thermal expansion of single wall carbon nanotubes. *J. Eng. Mater. Technol.* **126**, 265–270 (2004).
29. Nikolaev, P. *et al.* Gas-phase catalytic growth of single-walled carbon nanotubes from carbon monoxide. *Chem. Phys. Lett.* **313**, 91–97 (1999).
30. Ruan, W. Z., Wang, Z. Y., Li, Y. C. & Liu, L. T. *In-situ* heat capacity measurement of carbon nanotubes using suspended microstructure-based microcalorimetry. *IEEE Trans. Nanotechnol.* **11**, 367–373 (2012).
31. Fujii, M. *et al.* Measuring the thermal conductivity of a single carbon nanotube. *Phys. Rev. Lett.* **95**, 065502 (2005).
32. Barone, P. W., Baik, S., Heller, D. A. & Strano, M. S. Near-infrared optical sensors based on single-walled carbon nanotubes. *Nat. Mater.* **4**, 86–92 (2005).
33. Timoshenko, S. Analysis of bi-metal thermostats. *J. Opt. Soc. Am.* **11**, 233–255 (1925).

### Acknowledgements

We thank A. Majumdar for supporting the thermal conductivity measurements. This work was supported by the NSF Center of Integrated Nanomechanical Systems. Wave-length-dependent measurements were performed in the Electronic Materials Program, LBNL, which is supported by the Director, Office of Science, Office Basic Energy Sciences, Division of Materials Sciences and Engineering, of the US Department of Energy under Contract No. DE-AC02-05CH11231. A.D.B. and R.S.F. acknowledge Darpa M3 funding. M.C.H. acknowledges funding from the National Science Foundation (DMR-1006391).

### Author contributions

X.Z. and A.J. designed the experiments. X.Z., Z.Y., C.W., D.Z., J.C.C., A.D.B., K.T., M.H., J.W.A. and J.Z. carried out the photoactuator experiments. X.Z., D.Z., Z.Y. and R.S.F. performed mechanical modelling. Y.Z. performed thermal conductivity measurements. J.C.C., X.Z., D.Z. performed infrared imaging measurements. J.-W.T.S., M.C.H. performed nanotube chirality purification. X.Z., C.W., Z.Y., D.Z., R.S.F. and A.J. contributed to analysing the data. X.Z., C.W. and A.J. wrote the paper while all authors provided feedback.

### Additional information

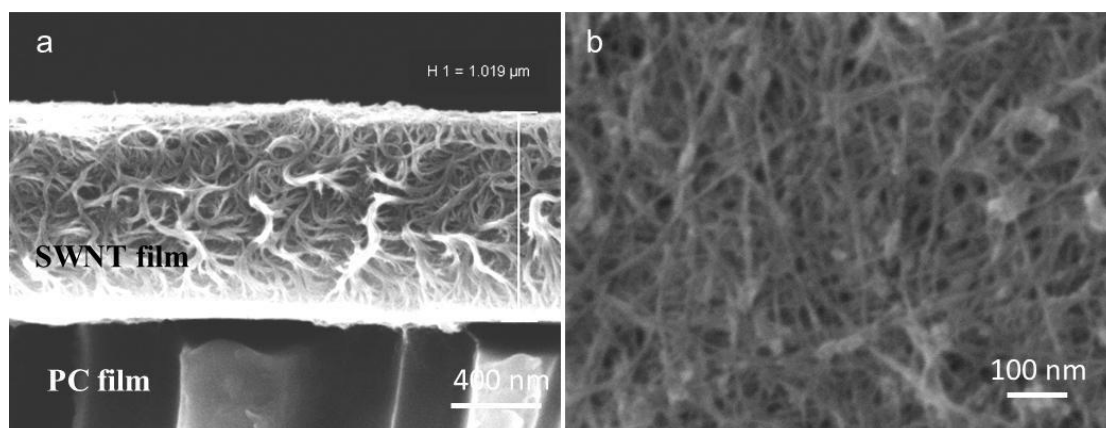
**Supplementary Information** accompanies this paper at <http://www.nature.com/naturecommunications>

**Competing financial interests:** The authors declare no competing financial interests.

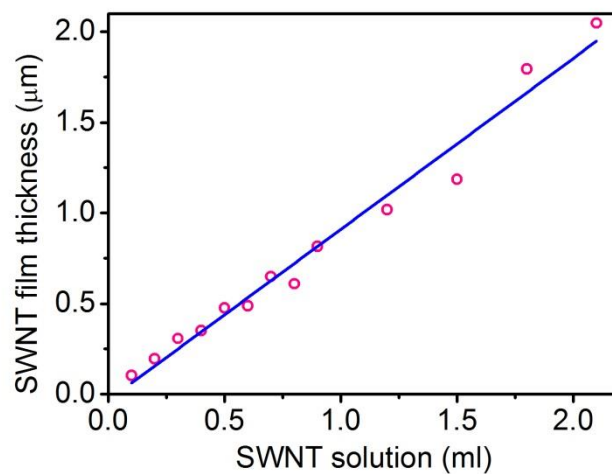
**Reprints and permission** information is available online at <http://npg.nature.com/reprintsandpermissions/>

**How to cite this article:** Zhang, X. *et al.* Photoactuators and motors based on carbon nanotubes with selective chirality distributions. *Nat. Commun.* **5**:2983 doi: 10.1038/ncomms3983 (2014).

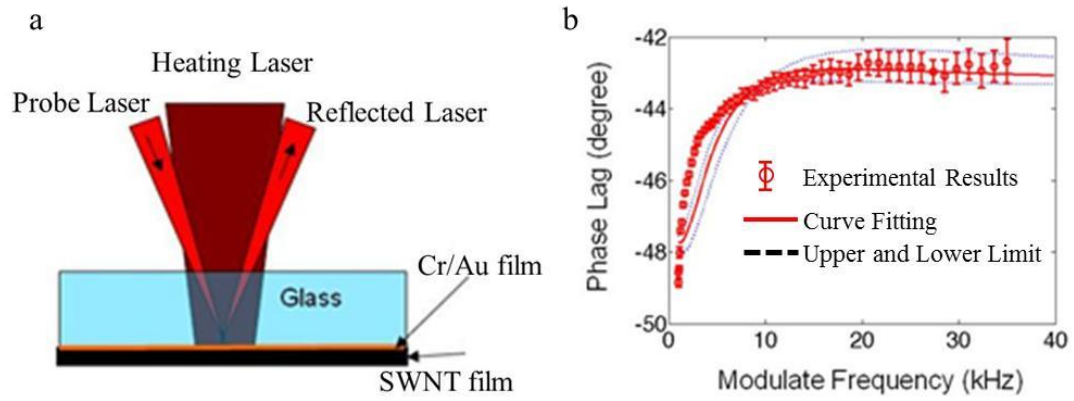
## Supplementary Figures



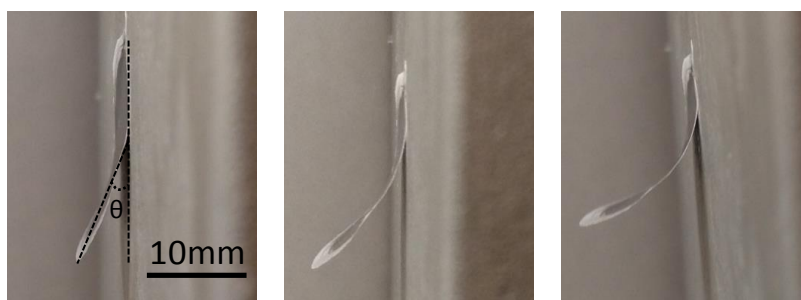
**Supplementary Figure S1.** **a**, the cross-sectional and **b**, top view SEM images of a PC/SWNT bilayer (SWNT film thickness of  $\sim 1 \mu\text{m}$ ).



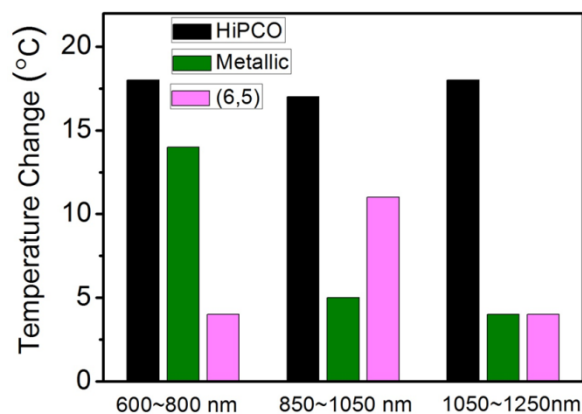
**Supplementary Figure S2.** The obtained SWNT film thickness versus the amount of SWNT solution (~0.5 mg/ml) used for vacuum filtration. The thickness of the SWNT thin film can be linearly controlled by the amount of SWNT solution used for vacuum filtration.



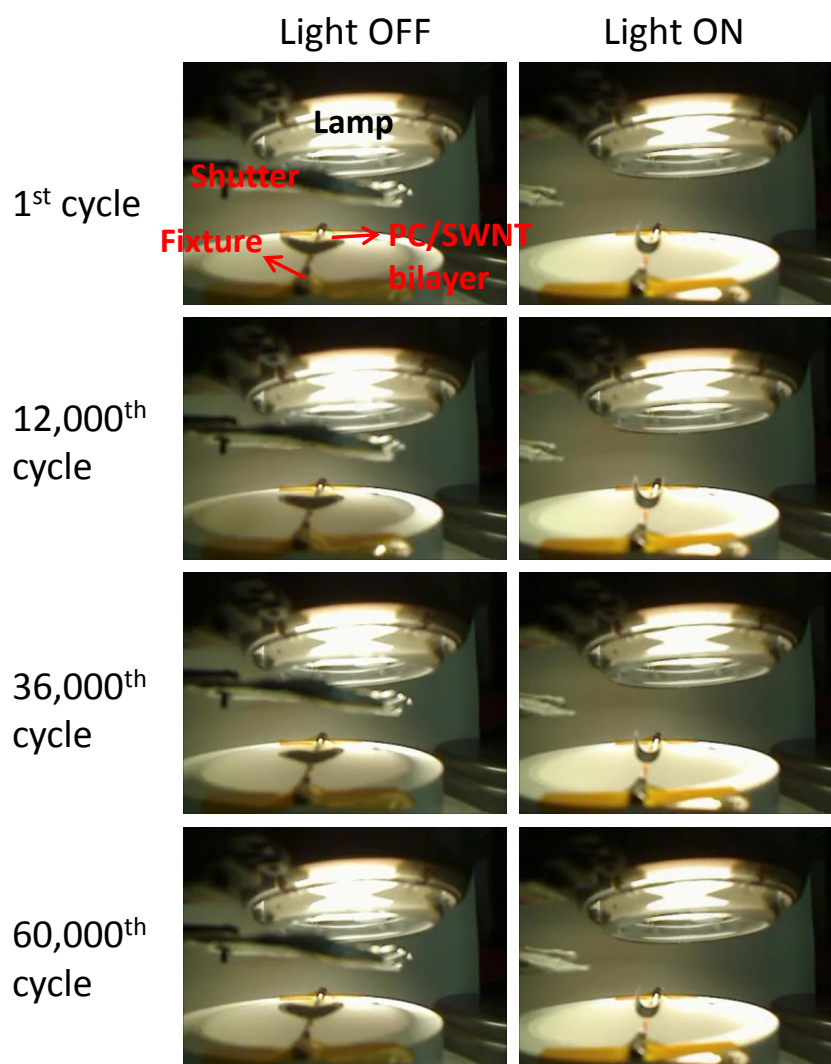
**Supplementary Figure S3. a**, Experimental configuration for SWNT film thermal conductivity measurements. **b**, Phase sensitive transient thermal reflectance (PSTTR) experimental data and curve fitting.



**Supplementary Figure S4.** Thermal actuation of a bilayer placed inside an oven (from left to right:  $\Delta T=5, 9$  and  $13$  °C). PC/SWNT bilayers were placed inside an oven at varied temperatures to examine the actuation induced by pure thermal effects. The temperature of the oven was varied and the actuation bending angle of the bilayer was measured. The measured bending angles for the thermal actuation are consistent with those obtained from photothermal actuation experiments for the same temperature change,  $\Delta T$  (in respect to the room temperature of  $\sim 25$  °C). This data is summarized in the Supplementary Table S2.



**Supplementary Figure S5.** Maximum temperature change for bilayers made with nanotubes of different chirality distributions, when illuminated with different wavelength bands of 600-800 nm, 850-1050 nm, and 1050-1250 nm. For each wavelength band, the light source is calibrated to maintain the same transmitted power of  $\sim 35 \text{ mW/cm}^2$ .



**Supplementary Figure S6.** Optical images of a PC/SWNT bilayer actuator under light (right) and dark (left) for multiple cycles of actuation. An automated shutter is used to expose the bilayer to white light with a cycle frequency of 0.5 Hz (shutter is opened for 1 sec and closed for 1sec per cycle). Snapshots showing the actuation for the 1<sup>st</sup>, 12,000<sup>th</sup>, 36,000<sup>th</sup>, 48,000<sup>th</sup> and 60,000<sup>th</sup> cycles are shown. The photo-induced deformation and bending angle remained unchanged as a function of actuation cycle. This work clearly shows the operation robustness of the actuators. Supplementary Movie S5 is also provided that shows 1,200 cycles of actuation for a bilayer.

## Supplementary Tables

(a)

<b>CNT film thickness (<math>\mu\text{m}</math>)</b>	.195	.477	.816	1.08	1.35	1.734	2.05
<b>Max dT (<math>^{\circ}\text{C}</math>)</b>	8.7	10.7	9.4	10.0	10.6	10.1	12.3

(b)

<b>CNT film thickness (<math>\mu\text{m}</math>)</b>	.195	.477	.816	1.08	1.35	1.734	2.05
<b>Max dT (<math>^{\circ}\text{C}</math>)</b>	6.4	6.4	6.8	7.2	7.4	8.4	8.0

**Supplementary Table S1.** Measured temperature change for SWNT/PC bilayers with different SWNT thicknesses upon **a**, 0.4 sun ( $40 \text{ mW}/\text{cm}^2$ ) and **b**, 0.3 sun ( $30 \text{ mW}/\text{cm}^2$ ) light illumination. PC film thickness is  $10 \mu\text{m}$  for all cases.

$\Delta T$ ( $^{\circ}\text{C}$ )	Maximum bending angle, $\theta$ (degrees)	
	Thermal	Photo Irradiation
5	21 $^{\circ}$	20 $^{\circ}$
9	36 $^{\circ}$	40 $^{\circ}$
13	54 $^{\circ}$	59 $^{\circ}$

**Supplementary Table S2.** Comparison of photothermal and thermal actuation of a PC/SWNT bilayer placed inside an oven (from left to right:  $\Delta T=5, 9$  and  $13$   $^{\circ}\text{C}$ ); temperature increases are in respect to the room temperature ( $\sim 25$   $^{\circ}\text{C}$ ) caused by thermal or photothermal heating.

## Supplementary Notes

### Supplementary Note 1

#### Calculated thermal response time of the PC/SWNT film

Thermal conductivity of SWNT films is measured with the Phase Sensitive Transient Thermal Reflectance (PSTTR) method. The experimental configuration is shown in Supplemental Figure S3a. A free standing SWNT film is obtained by dissolving the PC filtration membrane in dichloromethane. The SWNT thin film is then transferred onto a 0.5 mm thick glass substrate. The glass substrate has a thin film of Cr/Au (10nm/100nm) coating. The intensity of the heating laser is modulated at a frequency  $\omega$ . The surface temperature fluctuates with the heating power but with a phase lag due to the thermal impedance of the sample. The intensity of the reflected probe laser is modulated by the surface temperature due to thermo reflectance effect. A lock-in amplifier is used to capture the fluctuation of the intensity of the probe laser and record the phase lag, which is determined by the thermal properties of the sample. The modulation frequency is swept from 1 kHz to 35 kHz. The measured phase lag along with the modulation frequency is plotted in Supplemental Figure S3b. The thermal conductivity of the SWNT film is extracted by curve fitting based on the heat conduction model of the sample. The solid line in Supplemental Figure S3b is the fitted curve, corresponding to a thermal conductivity of the nanotube film of 0.07 W/m-K. The dashed lines in Supplemental Figure S3b show the upper and lower limits of the thermal conductivity, which are 0.12 W/m-K and 0.05 W/m-K, respectively.

To determine the heat transfer coefficient of the PC/SWNT bilayer, we assume the heat transfer coefficients of free air convection on the two surfaces of PC/SWNT structure are the same. As shown in Figure 2c, at 0.3 sun intensity, the maximum temperature change of the PC/SWNT film is 7.2°C. At steady-state we have

$$2h\Delta T = W_{in}$$

where  $h$  is the average heat transfer coefficient of free air convection at the two PC/SWNT surfaces;  $\Delta T$  is the temperature difference between the PC/SWNT film and ambient room temperature.  $W_{in}$  is the input power incident on the PC/SWNT bilayer. From this equation we can get  $h \sim 20.6 \text{ Wm}^{-2}\text{K}^{-1}$ .

From the obtained SWNT film thermal conductivity and the SWNT film thickness of 1 $\mu\text{m}$ , we can calculate the Biot number of the SWNT film to be on the order of  $10^{-4}$ , which is much smaller than 1. Therefore, the SWNT film can be considered isothermal. On the other hand, the thermal conductivity of the PC film is around  $0.19 \text{ W/m-K}^{34}$  with a thickness of 10  $\mu\text{m}$ . The calculated Biot number of the PC film is on the order of  $10^{-3}$  which is also much smaller than 1. Therefore the PC film can also be considered isothermal. The thermal time constant associated with the SWNT film only is then determined by the boundary conditions and the thermal mass of the film:

$$\tau = \rho C b / h$$

where  $\rho$  (1500  $\text{kg/m}^3$ ) is mass density of the film,  $C$  (= 550  $\text{J/kg-K}$ ) the specific heat of SWNTs<sup>35</sup>,  $b$  (= 1.0  $\mu\text{m}$ ) the thickness of the film, and  $h$  (= 20.6  $\text{W/m}^2\text{-K}$ ) is the heat transfer coefficient of free air convection at the boundary. Given the parameters above,

we estimate a thermal time constant of  $\sim 0.04$  second for the SWNT layer. For the PC film, the thermal response time can be calculated according to  $\tau = \rho C b / h$ , where  $\rho = 1200 \text{ kg/m}^3$  is mass density of the PC film<sup>36</sup>,  $C = 1200 \text{ J/kg-K}$  is the specific heat capacity of PC,  $b = 10.0 \text{ }\mu\text{m}$  is the thickness of the PC film, and  $h = 20.6 \text{ W/m}^2\text{-K}$  is the heat transfer coefficient at the interface. Given the parameters above, we calculate a thermal time constant of  $\sim 0.7$  second which matches our experimental value very well. The results suggest that the heat transfer in the PC layer is the limiting step in determining the response time of the system.

We note that the time response of the bending and unbending in the actual device operation could vary slightly depending on the specific set-up and how the actuator is thermally linked to the environment. For bending (i.e., upon light exposure), the response time is predominantly limited by the heat transfer coefficient at the bilayer interface as discussed above. On the other hand, for unbending (i.e., when light illumination is turned off), the response time is limited by how fast the heat is released to the surrounding environment. From Figure 1d, we observe that the time constant is roughly the same for bending and unbending. For this particular case, the bilayer is suspended in air and the heat loss during unbending is dominated by the heat transfer coefficient of free air convection at the surfaces.

## Supplementary Note 2

### Mechanical modeling for static maximum bending angle of PC/SWNT bilayers

At the initial stage of the photoactuation, light is incident normal to the surface of the sample which initiates the bending process. As a result of bending, the sample receives non uniform illumination which depends on the angle between the light and the locale surface normal direction (Figure 3a). Due to the small thickness of nanotube film (1  $\mu\text{m}$ ), the in-plane heat conduction is insignificant compared to free air convection. Therefore, the temperature of the sample at a specific point is predominantly a function of the incoming energy of the light and the convection coefficient  $h$  related by

- $$\dot{q} \cos(\theta) = 2h(T - T_{\text{air}})$$

where  $\theta$  and  $T$  are the bending angle and the temperature of the sample respectively at a local point,  $T_{\text{air}}$  is the room temperature, and  $\dot{q}$  is the energy input per area absorbed by the local area of the sample. Based on S. Timoshenko's bimetal beam thermostat model, the bending radius is

- $$\rho = \frac{h \left( 3(1+m)^2 + (1+mn) \left( m^2 + \frac{1}{mn} \right) \right)}{6(\alpha_2 - \alpha_1)(1+m)^2} \frac{1}{(T - T_0)} = \frac{C_{\text{Tim}}}{(T - T_0)}$$

$T_0$  is the room temperature at which the sample is flat. We denote the numerator of equation 2 by  $C_{\text{Tim}}$ . Inserting eq. 1 into eq. 2, we can get

- $$\rho = \frac{C_{\text{Tim}}}{(T - T_0)} = \frac{2hC_{\text{Tim}}}{\dot{q} \cos(\theta)}$$

For a small section of the sample, the bending angle of the end point relative to the start point is related to the bending radius through:

$$4. \quad \Delta\theta = \frac{\Delta L}{\rho}$$

Inserting eq. 3 into eq. 4, we obtain

$$5. \quad \Delta\theta = \frac{\dot{q} \cos(\theta) \Delta L}{2hC_{Tim}}$$

For infinitesimally small section of the sample  $dL$ , eq. 5 can be rewritten as

$$6. \quad \frac{d\theta}{dL} = \frac{\dot{q}}{2hC_{Tim}} \cos(\theta)$$

Solving the differential equation using Mathematica with boundary condition  $\theta(0) = 0$ , we can eventually get the bending angle at the tip:

$$7. \quad \theta(L) = 2\text{atan}\left(\tanh\left(\frac{\dot{q}L}{4hC_{Tim}}\right)\right)$$

As shown in the equation above, the bending angle is directly related to the total film thickness  $h$  (11  $\mu\text{m}$ ), the SWNT / PC thickness ratio  $m$  and Young's modulus ratio  $n$ , the maximum temperature change  $t-t_0$ , and the linear coefficient of thermal expansion (CTE) of PC  $\alpha_2$  (60 ppm/K)<sup>37</sup> and SWNT film  $\alpha_1$  (3 ppm/K)<sup>38</sup>. The modeling results match with the experimental results well (Fig. 3b) when the SWNT/PC Young's modulus ratio is set to 7.4 (Fig. 3b). The corresponding Young's modulus of SWNT film is consistent with previous reports<sup>39,40,41,42</sup>.

## Supplementary Note 3

### Calculated conversion efficiency of the photoactuators

The conversion efficiency of the bilayer photoactuators can be defined as the generated elastic energy due to photo-actuation divided by the incident light energy. The elastic energy density for our actuators can be approximated using the model previously developed for a bilayer bending beam as depicted in equation (1)<sup>43</sup>:

$$Energy = \frac{[E_s H_s^2 (3H_f + H_s) + E_f H_f^2 (3H_s + H_f)] \times [E_f^2 H_f^4 + E_s^2 H_s^4 + 2E_f E_s H_f H_s (2H_f^2 + 2H_s^4 + 3H_f H_s)]}{36E_f E_s H_f^2 H_s^2 (H_s + H_f)} k^2 \quad (1)$$

where the subscripts  $f$  and  $s$  represent the SWNT film and PC substrate layers, respectively.  $E$  is the Young's modulus,  $H$  is thickness and  $k$  is bending curvature.

The parameters for the above equation are listed below:

$$E_s = 2 \times 10^9 \text{ Pa}; E_f = 1.5 \times 10^9 \text{ Pa}; H_s = 1 \times 10^{-5} \text{ m}; H_f = 1 \times 10^{-6} \text{ m}$$

At 100 mW/cm<sup>2</sup> white light illumination, the bending radius is ~0.5cm, corresponding to  $k = 200 \text{ m}^{-1}$ . The calculated elastic energy density is then 6120 J/m<sup>3</sup>, corresponding to a total elastic energy of ~3×10<sup>-5</sup> J. Assuming an actuation time of ~0.7 sec, the total light energy exposed on the SWNT/PC bilayer for a single actuation cycle with 100 mW/cm<sup>2</sup> illumination is ~0.3 J. The conversion energy efficiency is then calculated to be ~ 0.01%

## Supplementary References

---

- <sup>34</sup> King J. A., Via M. D., King M. E., Miskioglu I., & Bogucki G. R., Electrical and Thermal Conductivity and Tensile and Flexural Properties: Comparison of Carbon Black/Polycarbonate and Carbon Nanotube/Polycarbonate Resins, *J. Appl. Polym. Sci.*, **121**, 2273-2281, (2011)
- <sup>35</sup> Yi, W., Lu, L., Zhang, D., Pan, Z. W., & Xie, S. S., Linear specific heat of carbon nanotubes, *Phys. Rev. B*, **59**, R9015, (1999)
- <sup>36</sup> Ito Y., Yamashita M., & Okamoto M., Foam processing and cellular structure of polycarbonate-based nanocomposites, *Macromol. Mater. Eng.*, **291**, 773-783, (2006)
- <sup>37</sup> Sung Y. T. *et al.*, Properties of polycarbonate/acrylonitrile-butadiene-styrene/talc composites, *J. Appl. Polym. Sci.*, **124**, 1020-1030, (2012)
- <sup>38</sup> Alamusi *et al.*, Prediction of thermal expansion properties of carbon nanotubes using molecular dynamics simulations, *Comput. Mater. Sci.*, **124**, 249-254, (2012)
- <sup>39</sup> Hakimelahi H. R., Hu L., Rupp B. B., & Coleman M. R., Synthesis and characterization of transparent alumina reinforced polycarbonate nanocomposite, *Polymer*, **51**, 2494-2502, (2010)
- <sup>40</sup> Berhan L. *et al.*, Mechanical properties of nanotube sheets: Alterations in joint morphology and achievable moduli in manufacturable materials, *J. Appl. Phys.*, **95**, 4335-4345, (2004)
- <sup>41</sup> Sreekumar T. V. *et al.*, Single-wall carbon nanotube films, *Chem. Mater.*, **15**, 175-178, (2003)
- <sup>42</sup> Coleman J. N. *et al.*, Improving the mechanical properties of single-walled carbon nanotube sheets by intercalation of polymeric adhesives, *Appl. Phys. Lett.*, **82**, 1682-1684, (2003)
- <sup>43</sup> Merced, E., Tan, X., & Sepulveda, N. Strain energy density of VO<sub>2</sub>-based microactuators. *Sensors and Actuators A: Physical*, **196**, 30-37, (2013)